Electrical and Optical Properties of Rutile Single Crystals*

D. C. CRONEMEYER†
Laboratory for Insulation Research, Massachusetts Institute of Technology, Cambridge, Massachusetts
(Received January 9, 1952)

Clear, synthetic rutile (TiO_2) single crystals have been investigated by electrical and optical methods. It seems possible to correlate the high temperature conductivity ($E_G=3.05$ ev) with the threshold of optical absorption at low temperatures (3.03 ev) and with the maximum of the photoconductivity (3.03–3.06 ev). This evidence indicates an energy gap *ca* 3.05 ev for rutile as an insulator.

Semiconducting rutile, prepared by hydrogen reduction at temperatures $\leq$800°C, shows a blue color arising from an optical absorption maximum at *ca* 1.7μ (0.73 ev). Conductivity-temperature plots for slightly reduced specimens indicate an optical activation energy of 0.68 ev. A theoretical calculation for the ionization of the first electron from an oxygen vacancy indicates 0.74 ev as the expected value, in good agreement with the experimental results. At room temperature the mobility of electrons in slightly reduced single crystals is *ca* 10^{-4} m²/v-sec.

Strongly reduced rutile is opaque; a comparison of electron concentrations calculated from weight loss and Hall coefficient data shows that for samples in which the electron concentration is 10^{26}/m³, all contribute to conduction at room temperature.

INTRODUCTION

TWO major projects of the Laboratory for Insulation Research are concerned with long-range studies on (1) transition stages from insulators to semiconductors to metals, and (2) dielectrics of high dielectric constant, especially ferroelectrics. Rutile TiO_2 occupies a key position in both projects since it is a basic constituent of the ferroelectric titanates, and the series TiO_2-Ti_2O_3-TiO-Ti is an interesting oxide system in which a progressive transition from insulator to metal is accomplished by reduction.[1] Finally, TiO_2 itself has much higher dielectric constants and indices of refraction than most crystals and a large dielectric anisotropy.[2–5] Therefore, new information concerning the characteristic behavior of electrons in a medium of high electronic and atomic polarizability can be obtained.

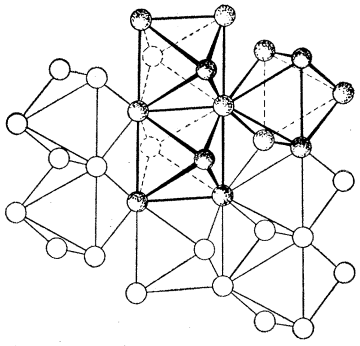

FIG. 1. Octahedra-packing diagram for rutile TiO_2.

The Laboratory has studied TiO_2 in some respects,[6–8] but its investigations until now have been limited to ceramic samples since the natural rutile crystals are usually impure. Recently, colorless large single crystals of synthetic rutile have been grown by the boule technique.[9] Therefore, the present research was undertaken to establish the fundamental electrical and optical properties of these crystals and the changes occuring upon reduction.

The rutile-TiO_2 crystal is composed of titanium and oxygen in their highest valence states +4 and −2, respectively. Titanium is a transition metal of the iron group, the normal atomic electronic configuration of which is $(4s)^2(3d)^2$ outside the argon core.[10] In the periodic system the place of titanium is just beyond the point in the iron transition group where the 4*s* shell is filled and it becomes easier to put the next electron into a 3*d* shell than into the 4*p* shell.[11] This fact might lead to an *s-p-d* hybridization resulting in a sixfold oxygen co-ordination, which may be described as the formation of a TiO_6 octahedron. Likewise, from the standpoint of a purely ionic structure, the radius ratio of Ti^{+4} to O^{-2} would lead one to expect a sixfold co-ordination of Ti with O.[12] In the rutile crystal each octahedron shares two of its edges with other octahedra while each of the remaining two free corners is shared with two other octahedra[13] (Fig. 1).

* Sponsored by the ONR, the Army Signal Corps, and the Air Force under ONR contract N5ori-07801.

† Present address, General Electric Company, Syracuse, New York.

[1] P. Ehrlich, Z. Elektrochem. **45**, 362 (1939).
[2] A. Schröder, Z. Krist. **67**, 485 (1928).
[3] T. Liebisch and H. Rubens, Sitzber. preuss. Akad. Wiss., Physik.-math. Kl. 211 (1921).
[4] W. Bärwald, Z. Krist. **7**, 168 (1883).
[5] C. W. Carstens, Z. Krist. **67**, 261 (1928).
[6] A. von Hippel *et al.*, "High Dielectric Constant Ceramics I and II," Lab. Ins. Res., N.D.R.C. Reports No. 300 (1944); 540 (1945).
[7] von Hippel, Breckenridge, Chesley, and Tisza, Ind. Eng. Chem. **38**, 1097 (1946).
[8] A. von Hippel, Revs. Modern Phys. **22**, 221 (1950).
[9] We are greatly indebted to Dr. C. H. Moore of the National Lead Company for the specimens used in this research.
[10] J. C. Slater, *Introduction to Chemical Physics* (McGraw-Hill Book Company, Inc., New York, 1939), p. 346.
[11] G. Herzberg, *Atomic Spectra and Atomic Structure* (Dover Publications, New York, 1944), p. 148.
[12] L. C. Pauling, *The Nature of the Chemical Bond* (Cornell University Press, Ithaca, 1948).
[13] R. W. G. Wyckoff, *Crystal Structures Handbook* (Interscience Publishing Company, New York, 1948).

This construction of the rutile crystal can be shown to be more stable than that of the other two modifications of TiO_2, brookite and anatase, where three and four edges of each octahedron are shared, respectively.[14] The density of the crystals,[2] anatase, brookite and rutile, progresses from 3.9 to 4.12 to 4.22 g/cm^3 in accord with the fact that the dense rutile is the most stable form. The two other modifications are transformed into rutile upon heating near 1000°C. Within a TiO_6 group in rutile, the oxygen engaged in edge-sharing of this octahedron with two others have a bond distance of 1.89A from the central titanium ion, while the remaining two oxygens are found at the somewhat greater distance of 1.97A.

The assumption of completely ionic binding would make a regular octahedron the basic building block of TiO_2. With this assumption, Born and Bollnow[15] carried out a Madelung calculation for rutile which relates the electrostatic potential to the axial ratio c/a of the tetragonal unit cell. That analysis predicts an axial ratio c/a=0.721 for a maximum Madelung constant. In the actual crystal this would result in a too short O–O distance and the axial ratio[13] observed is c/a=0.644.

The failure of a purely ionic calculation to predict the correct c/a ratio and unequal Ti-O distances extends also to the magnitudes and temperature coefficients of the dielectric constants and refractive indices. It seems probable[16] that TiO_2 represents a transition between polar and nonpolar binding. Kirkwood[17] and Bartholomé[18] have made approximate calculations applying to such intermediate cases which show the change of dipole moment with internuclear separation. This change of dipole moment results in a negative temperature coefficient of the dielectric constant and refractive index.[2,6,19] Instead of visualizing octahedra, one may refer to chains of Ti-O-O-Ti-O-O-Ti ions,[20] alternate layers running perpendicular to one another throughout the crystal and oriented normal to the *c* axis. There is no tendency toward cleavage. The picture of Ti-O chains permits one to interpret the reststrahl vibrations as deformation and valence vibrations.[6] The Ti-O chains are so situated in the crystal that only a deformation vibration is excited by light with its *E* vector ∥ to the *c* axis (extraordinary ray), while light with its *E* vector ⊥ to the axis excites a combination of deformation and valence vibrations.[21] The optical dielectric constants[3] are: $(2.40)^2\perp$, $(2.57)^2\parallel$. Beyond the reststrahl region[3] the values of the dielectric constant at 300 μ approach those for static measurements,[3] namely 83 ⊥, 167 ∥ (Fig. 2).

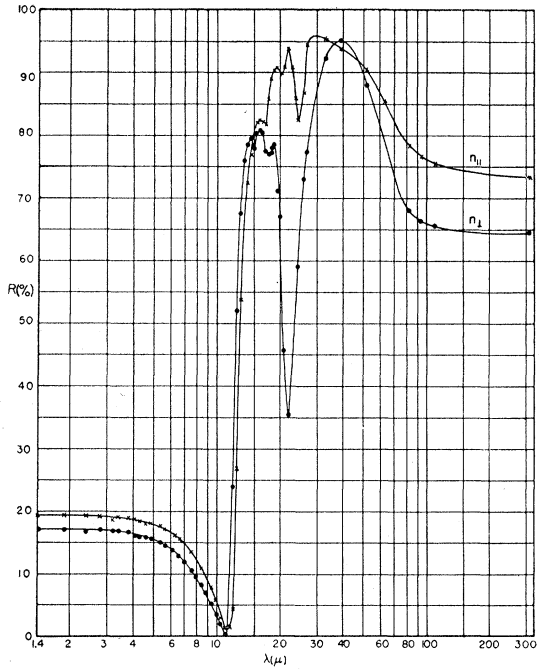

FIG. 2. Reflection coefficient in percent for rutile TiO_2 natural single crystals. Data from Liebisch and Rubens, reference 3.

THE INTRINSIC ELECTRICAL AND OPTICAL PROPERTIES OF RUTILE SINGLE CRYSTALS

Sample Preparation

Two samples of synthetic rutile were obtained in the form of boules, oriented by their x-ray Laue patterns, and sliced parallel and perpendicular to the *c* axis with a diamond wheel (accuracy *ca* 1°). After polishing, the first boule (*I*) showed several lineage flaws under the polarization microscope, with regions differing in extinction position by a degree or two. The second boule was a perfect single crystal with the exception of a small region on one face. Several prismatic bars *ca* 1×1×10 mm were cut from slices of boule *II* for the high temperature conductivity measurements; optical transmission measurements were made on polished plates.

High-Temperature Conductivity

Figure 3 shows one of the sample holders for high temperature conductivity measurements. Its construction has the advantage that the quartz holder extends outside the furnace into the room-temperature zone; hence the leakage is small and independent of the sample temperature. The temperature control of the furnace allowed maintenance of the temperature to *ca*±0.1° at 1000°C over long periods.

[14] L. Pauling, Z. Krist. **67**, 377 (1928).
[15] M. Born and O. F. Bollnow, Naturwiss. **13**, 559 (1925).
[16] A. Eucken and A. Büchner, Z. physik. Chem. **B27**, 321 (1934).
[17] J. G. Kirkwood, Physik. Z. **33**, 259 (1932).
[18] E. Bartholomé, Z. physik. Chem. **B23**, 131 (1933).
[19] E. Bretscher, Trans. Faraday Soc. **30**, 684 (1934).
[20] M. Born, *Dynamik der Kristallgitter* (Teubner, Leipzig, 1915); *Atomtheorie des festen Zustandes*, Encl. d. math. Wissenschaften V 3, 527 (1923); M. Born and M. Göppert-Mayer, *Dynamische Gittertheorie der Kristalle*, Handbuch der Physik **24**, 623 (1933).
[21] See also the case of UO_2 as discussed in P. Pringsheim, *Fluorescence and Phosphorescence* (Interscience Publishers, New York, 1949).

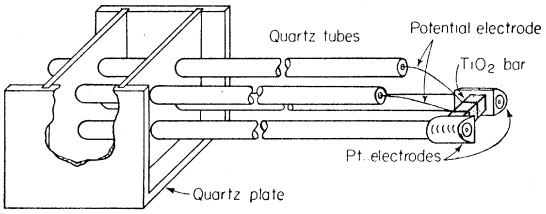

FIG. 3. High temperature sample holder.

The high temperature conductivity data for both crystal orientations fall on two straight lines which intersect at about 900°C (Figs. 4 and 5); about 200 points were measured for each characteristic to avoid ambiguous interpolation. The straight line for the conductivity $\perp$ to the c axis extends to lower temperatures than the line for the $\|$ orientation. The activation energies in ev derived from a Boltzmann equation $\sigma=\sigma_0\, e^{-\epsilon/kT}$ are: $\perp$, 1.53 at 350–850°C, 1.83 at 850–1400°C; $\|$, 1.53 at 500–950°C, 1.83 at 950–1400°C. Below *ca* 900°C the conductivity is field-strength sensitive for fields above 10^3 v/m (see insert of Fig. 4). The ac conductivity, measured at 100 cycles between 250° and 500°C checks the dc data almost exactly.

If the high temperature conductivity corresponds to an intrinsic electronic conduction, it follows from the band theory[22] that the actual gap width between the filled and the conduction band is twice the activation energy indicated on the previous logσ *vs* $1/T$ plot; i.e., $\sigma=\sigma_0 e^{-E_G/2kT}$. A tabulation of the constants σ_0 and E_G is given in Table I. A simple estimate of the values of σ_0 may be obtained by setting $\sigma_0=n_0eb$, where n_0 is the total number of valence electrons (4 per TiO_2), e is the electronic charge, and b the mobility in m²/v-sec. Since the number of TiO_2's per m³ is 3.18×10^{28}, $n_0=1.27\times10^{29}$/m³. In general, the mobilities for electrons

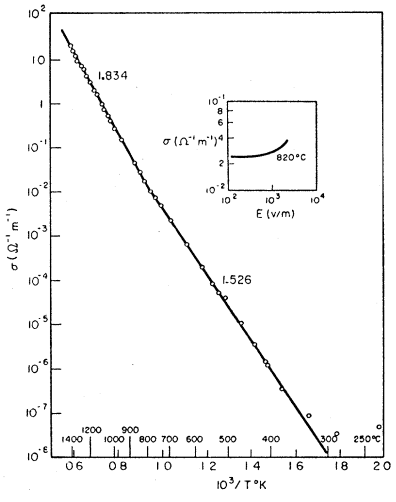

FIG. 4. High temperature conductivity-temperature plot for rutile $TiO_2\perp$ to c axis.

[22] A. H. Wilson, *Theory of Metals* (Cambridge University Press, Cambridge, 1936).

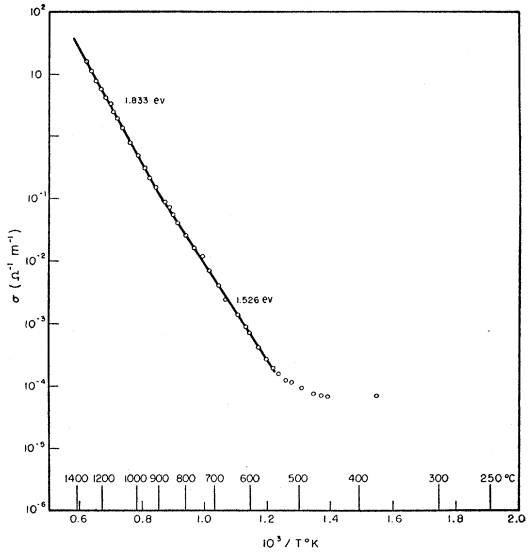

FIG. 5. High temperature conductivity-temperature plot for rutile $TiO_2\|$ to c axis.

in crystalline insulators at high temperatures are of the order of 10^3 to 10^5 m²/v-sec (0.1 to 10 cm²/v-sec); hence one obtains $\sigma_0=2\times10^5$ to 2×10^7 $\Omega^{-1}m^{-1}$ as the expected values in reasonable agreement with those of Table I.

That the conductivity is essentially electronic is evident from the fact that large currents can be passed for hours without destructive effect.

According to this interpretation of the high temperature conductivity, the optical eigenabsorption might be expected at 3.05 ev or 4070A.

The Optical Eigenabsorption and Associated Photoconductivity of Rutile

A quantitative study of the optical absorption edge of rutile single crystals requires index of refraction data near the edge for a calculation of the reflection loss. Such measurements were made on a small prism cut from a rutile single crystal (3 mm height, 3 mm face length, breaking angle 18°49′, c axis bisecting the base angle, and an a axis along the breaking edge). Figure 6 shows the results for the ordinary ray[23] in synthetic rutile as compared to the data of previous observers.[2,4] The refractive index measurements in the visible

TABLE I. Compilation of σ_0 and E_G values for rutile.

	$\sigma_0(\Omega^{-1}m^{-1})$	E_G(ev)	$\sigma_0(\Omega^{-1}m^{-1})$	E_G(ev)
($\|\|$)	4.59×10^5	3.05 (500–950°C)	8.38×10^6	3.67 (950–1400°C)
($\perp$)	2.76×10^5	3.05 (350–850°C)	6.82×10^6	3.67 (850–1400°C)
	$\frac{\sigma_{0\|\|}}{\sigma_{0\perp}}=1.66$		$\frac{\sigma_{0\|\|}}{\sigma_{0\perp}}=1.23$	

[23] The ordinary ray, often designated as n_0, is here indicated as n^* signifying that the E vector of the light is $\perp$ to the c axis of the crystal. Likewise, $n-$ denotes a wave with the E vector $\|$ to the c axis (the extraordinary ray).

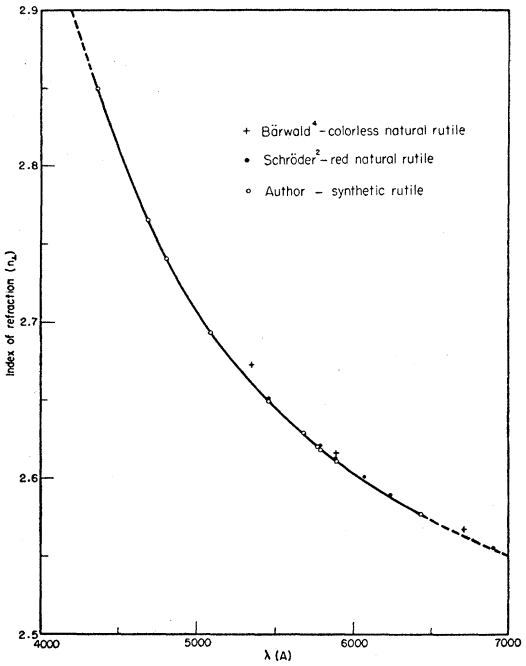

FIG. 6. Index of refraction, for the ordinary ray, of synthetic rutile TiO_2 compared with previous measurements for natural crystals.

region were extended into the infrared by calculation from reflection[3] and transmission curves (Fig. 7). Measurements of optical transmission in the visible range were made with a Cary recording spectrophotometer (Model 12-M, band width for the absorption edge, 5A).

A complete room-temperature transmission characteristic from 0.4 to 8μ is shown in Fig. 8. The infrared

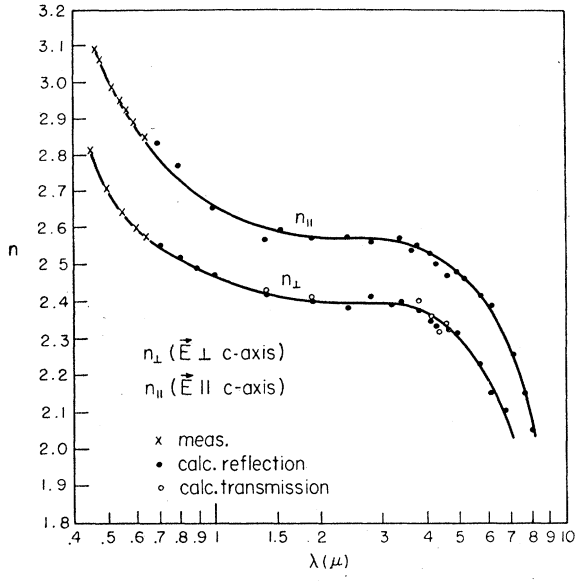

FIG. 7. Refractive index measurements extended by calculation from reflection (Liebisch and Rubens) and transmission.

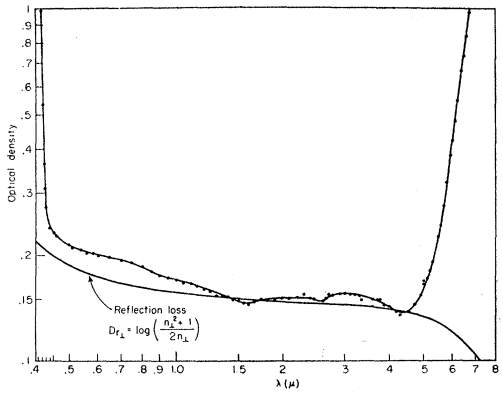

FIG. 8. Room-temperature optical transmission of 0.889-mm synthetic rutile plate cut normal to the optic axis.

transmission proves to be almost as large as the theoretical maximum calculated from refractive index data. The near-ultraviolet absorption edge appears quite sharp on this scale. Figure 9 shows the transmission in the visible region for a crystal cut parallel to the optic axis and measured with polarized light; the tail of the absorption appears considerably higher for the orientation ($\mathbf{E} \parallel c$) than the theoretical reflection loss justifies. This may be due to poor surface polish since plates having the optic axis in the plane are difficult to polish.

Thin film measurements have been made on evaporated layers of Ti formed on quartz after they were transformed to rutile by heating in air at 1000°C for several hours. The optical quality of such layers is so poor that curves are not given, but the room temperature maximum absorption is reached at 3.8 ev for an absorption coefficient of 5×10^7/m. The thickness determination from weighing and interference methods showed reasonable agreement.

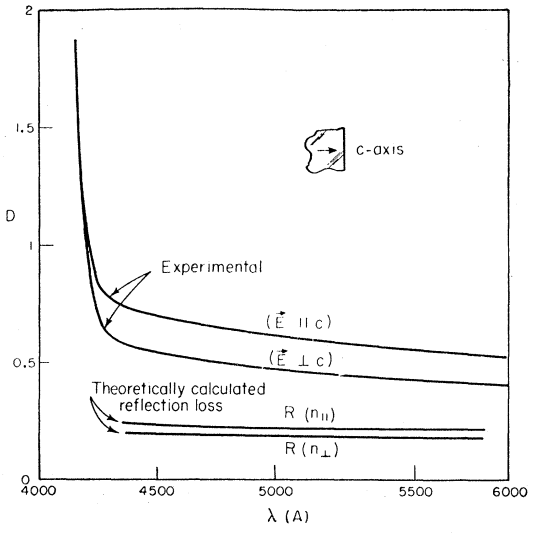

FIG. 9. Optical transmission of polarized light through 0.9-mm plate of synthetic rutile cut parallel to the optic axis.

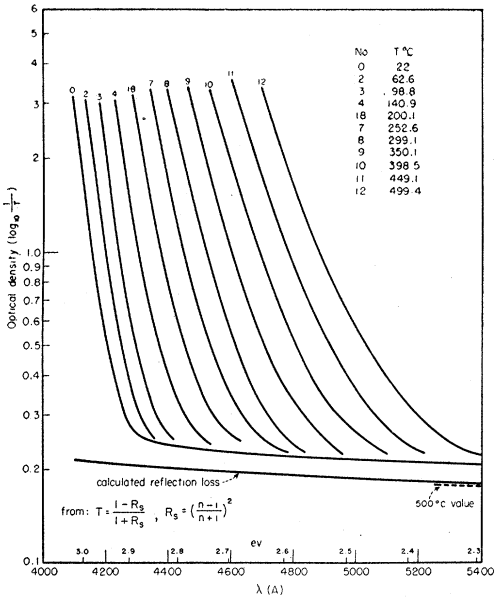

FIG. 10. Optical transmission (22–500°C) of 0.889-mm synthetic-rutile plate cut normal to the optic axis.

Reduction or oxidation affects the position of the optical absorption edge very little. Strong reduction moves the edge slightly to the red. Upon heating, the crystal turns greenish, then yellow and finally red at 800°C; the sequence is reversed upon cooling. The reason for this color change is evident from the optical density characteristics of Fig. 10. At 500°C the crystal is almost opaque to wavelengths shorter than green light, hence the crystal must appear amber by transmission.

The optical absorption edge sharpens toward low temperatures (Fig. 11) but exhibits, in addition, an unexpected shift toward longer wavelengths. To observe this behavior in more detail, measurements were carried out with higher resolution at temperatures

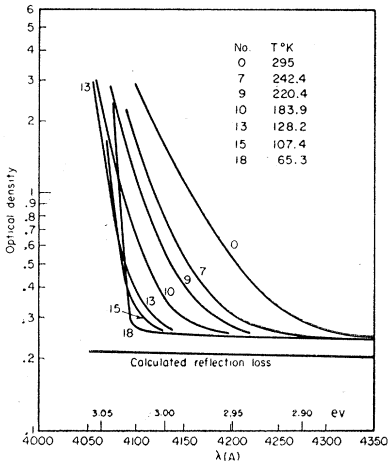

FIG. 11. Optical transmission (65–295°K) of 0.889-mm synthetic-rutile plate cut normal to the optic axis.

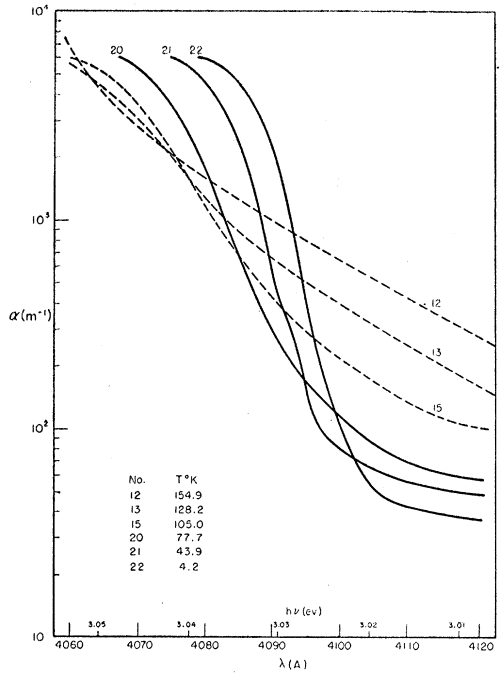

FIG. 12. Absorption coefficient of synthetic rutile TiO_2 normal to optic axis (derived from measurements on 0.889-mm plate).

between 65°K and the boiling point of liquid helium (4°K) (Fig. 12). It is seen that a secondary absorption separates from the fundamental absorption. Figure 13 combines measurements on two plates of different thickness in order to trace the characteristic into the region of high absorption.

The same crystal was clamped on a Vycor plate for photoconductivity measurements (Fig. 14). Graphite

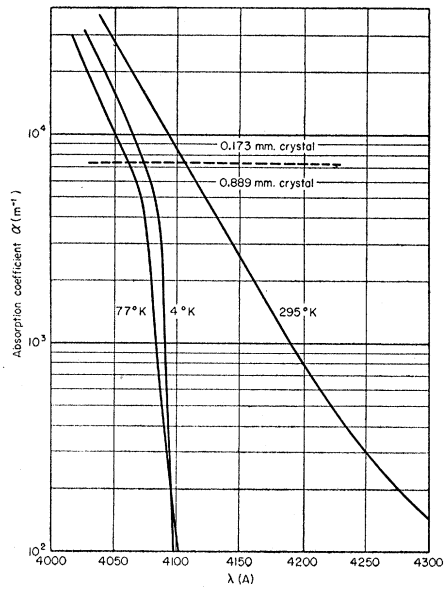

FIG. 13. Absorption coefficient (295–4°K) from a compilation of measurements on two crystals of synthetic rutile.

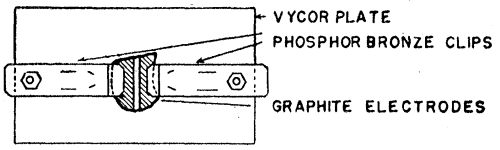

FIG. 14. Rutile crystal mounting for measurement of photoconductivity.

electrodes were applied to cover all of the face except for a central slit which exposed a single crystal region. The light, chopped at 60 cps, fell upon the sample through a quartz window. The data, corrected to constant incident energy, are shown in Fig. 15. Figure 16 shows the photocurrent for constant energy times quantum energy, i.e., the quantum yield, in arbitrary units, for several temperatures.

It may be noted that the maximum of the photoresponse moves toward shorter wavelengths with decreasing temperature paralleling the behavior of the optical absorption. At 100°K, a slight splitting into two peaks with a separation of about 0.1 ev is observed. A secondary maximum at 3.3 ev seems to be already in evidence at 230°K.

The long wavelength tail of the photoresponse has been measured to 1.2μ with modulated light (Fig. 17). There is some evidence that the response is still detectable to about 2μ, but these measurements were made uncertain by drift and long induction and decay times.

The optical band separation given by the edge of the eigenabsorption at low temperatures is 3.03 ev; from the high temperature conductivity it is 3.05 ev; and from the photoconductivity maximum it is 3.00 to 3.06 ev; an average value *ca* 3.05 ev is indicated.

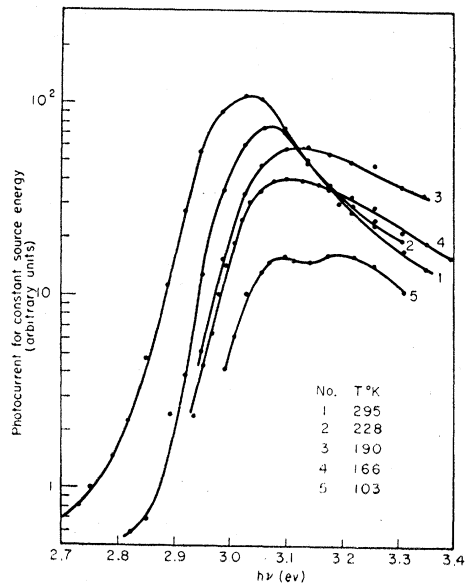

FIG. 15. Photocurrent response corrected to constant incident light intensity for rutile TiO_2.

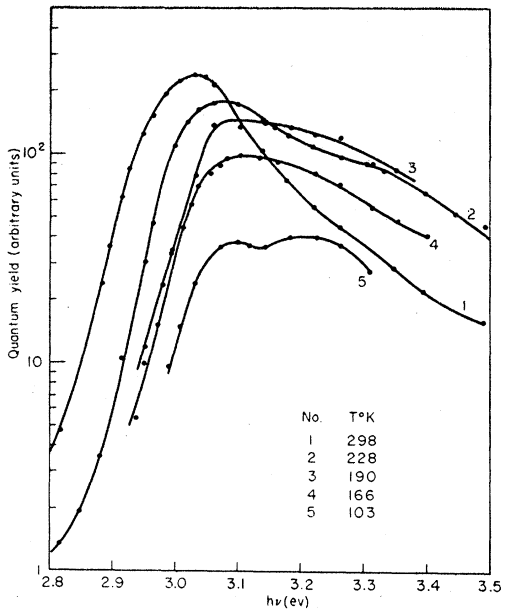

FIG. 16. Quantum yield *vs* $h\nu$ (ev) for rutile TiO_2.

OPTICAL ABSORPTION AND CONDUCTIVITY OF REDUCED SINGLE CRYSTALS

Slightly Reduced Crystals

Figure 18 compares the optical density expected from reflection loss only with the density actually measured on a clear crystal and on a slightly reduced crystal. In the nonreduced crystal the optical density in the visible range is already higher than the reflection loss; after traversing a broad maximum at *ca* 0.73μ, the discrepancy disappears at 1.5μ, and reappears with

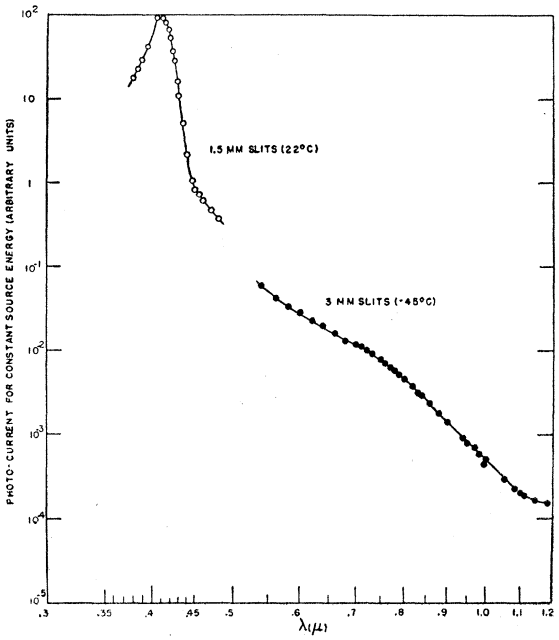

FIG. 17. Long wavelength photoresponse for rutile TiO_2.

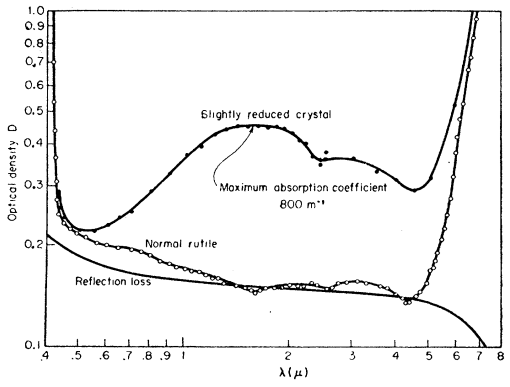

FIG. 18. Optical density *vs* wavelength for normal and slightly reduced rutile.

two slight maxima at 2.3 and 3.2μ. It is not certain that the minimum of optical density occurring at 2.55μ is characteristic of the crystal since this is the wavelength at which a change of infrared equipment had to be made. After reduction in hydrogen at 600°C until a faint blue color was discernible a broad peak, with its maximum at 1.85μ, is observed. In the reduced crystal photoconduction was observable to at least 2μ by dc techniques but no response maximum was clearly discerned for the peak of the optical absorption.

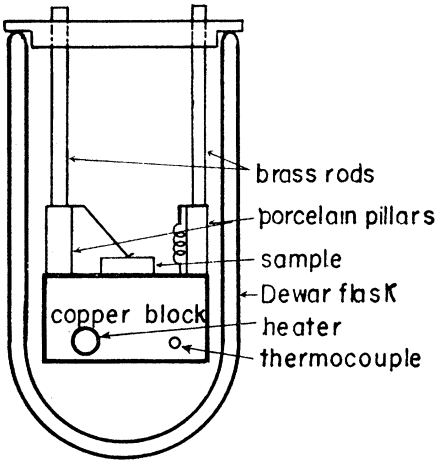

FIG. 19. Sample mounting for over-all conductivity measurement.

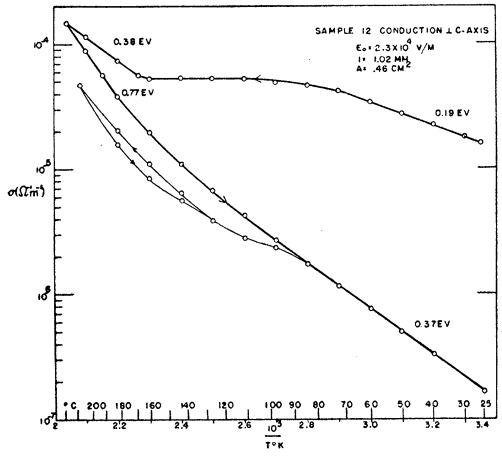

FIG. 20. Conductivity-temperature characteristic of rutile TiO_2.

To obtain the temperature dependence of the dark conductivity, gold electrodes were evaporated onto the samples. Since reduction increases the conductivity appreciably, a sample holder with thermostated silicone oil was used (Fig. 19) and the temperature taken to only *ca* 250°C. When a fairly low field was applied and the temperature raised, the $\log\sigma_0$ *vs* $1/T$ plot (Fig. 20) started at room temperature with a slope of 0.19 ev, leveled off at about 80°C, and at 160° rose again with a steeper slope. During cooling σ_0 followed an entirely different curve with a greater activation energy (0.37 ev). Upon repetition of the cycle (the lower loop in Fig. 20), the plateau of the curve almost disappeared, and the conductivity became nearly reproducible in subsequent warming and cooling cycles. For high field strength, on the other hand, the return trace was above the initial one and followed a straight line from 200°C to room temperature (Fig. 21).

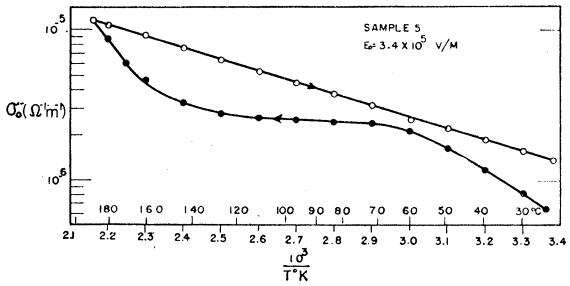

FIG. 21. Conductivity-temperature characteristic of rutile TiO_2.

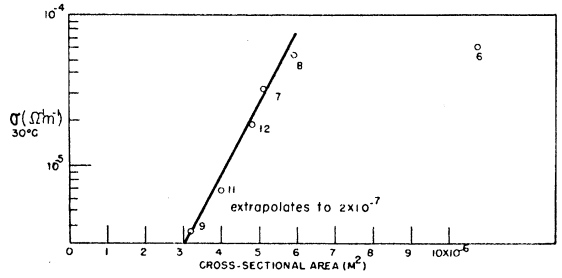

FIG. 22. Conductivity *vs* cross-sectional area for rutile TiO_2.

Figure 22 shows that the initial over-all conductivities of a number of samples appear to depend upon the cross-sectional area. This might result from the increased effectiveness of oil cooling for a slender sample, but more likely indicates carrier injection with predominant recombination at the surface of the sample.

After cooling in a high field, the slightly reduced crystal bars sometimes showed a concentration of the blue color at the cathode probably caused by a migra-

tion of the color centers (oxygen defect) toward the negative electrode.

The conductivity values as reported above might be misleading since the voltage distribution within the sample is not specified. Therefore, a determination of this distribution $V(x)$ was made with a platinum probe which traversed the surface of optically polished TiO_2 bars (*ca* $1\times1\times10$ mm). The probe potential with respect to both the anode and the cathode was determined with an electrometer in a null-type arrangement.

A typical $V_K(x)$ curve (Fig. 23) shows the field markedly distorted near the electrodes so that the net field in the central portion of the crystal (E) is appreciably smaller than the applied field strength (E_0). A variety of ratios of cathode- to anode-potential drops were obtained but all curves had the same general appearance. Figures 24(a) and (b) compare this true conductivity σ with the over-all conductivity σ_0 as

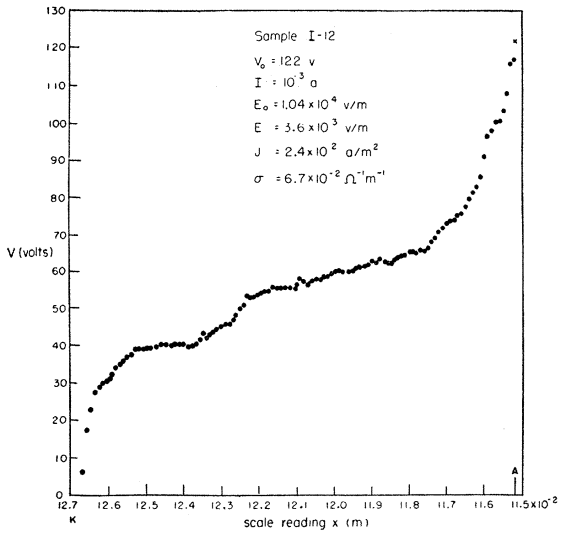

FIG. 23. Voltage-distribution curve illustrating the derivation of true conductivity σ compared with over-all conductivity σ_0.

a function of applied field and orientation. $V(x)$ curves taken for a constant applied voltage and variable temperature show that the field distortion disappears at about 90°C, and that above this temperature a slight distortion of the opposite character occurs.

Hall effect measurements were made using a sample holder, similar to that described by Hartmann,[24] with either a permanent magnet of 0.5 weber/m^2 or a Weiss magnet up to 1 weber/m^2 (10,000 gauss).

With a primary current of 800μ a parallel to the c axis of a crystal, measured in oil at room temperature, the characteristic of Fig. 25 was obtained. From the slope of the straight line ($V_H/B=1.46\times10^{-3}$ [v-m^2/weber]) we find the Hall constant $R=-2.26\times10^{-3}$ [m^3/coulomb], hence a concentration of electrons 3.3 $\times10^{21}$ m^{-3}. The conductivity was measured as σ

[24] W. Hartmann, Z. Physik **102**, 709 (1936).

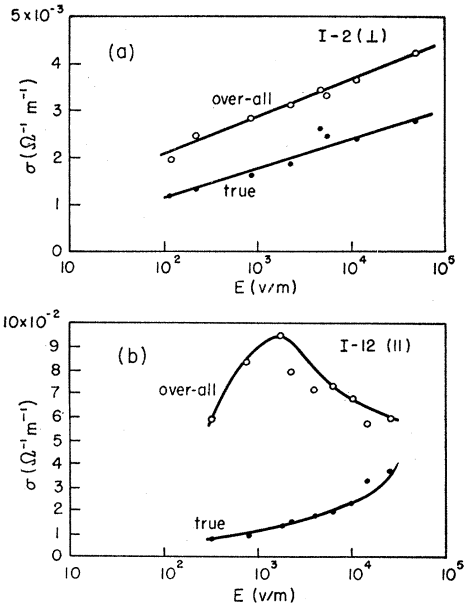

FIG. 24. True and over-all conductivity, σ and σ_0, for rutile crystals with the field (a) $\perp$ and (b) $\parallel$ to the c axis.

$=5.63\times10^{-2}\ \Omega^{-1}$ m^{-2}, hence the mobility b of the electrons is 1.1×10^{-4} m^2/v-sec (or 1.1 cm^2/v-sec).

It should be pointed out that this calculation is questionable since there are three possible orientations for Hall effect measurements in a tetragonal crystal, namely, (1) $I \parallel c$; (2) $I \perp c$, $B \perp c$; (3) $I \perp c$, $B \parallel c$. In bismuth single crystals, the Hall coefficients, and their temperature coefficients are different in all three directions.[25] There is also uncertainty regarding the interpretation of the Hall coefficients in an anisotropic crystal since the distribution of the energy surfaces within the Brillouin zone is required for a theoretical interpretation.[22,26–28] Unfortunately, time did not permit studying the directional Hall effect in rutile.

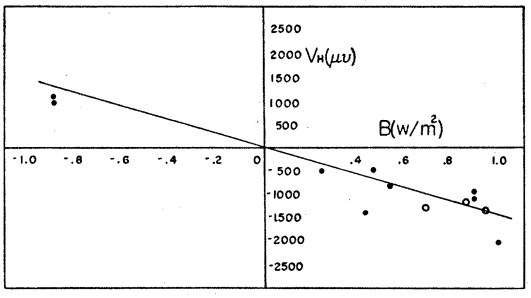

FIG. 25. Hall voltage *vs* magnetic induction ($I \parallel c$).

[25] A. F. Joffé, *The Physics of Crystals* (McGraw-Hill Book Company, Inc., New York, 1928).

[26] W. Shockley, *Electrons and Holes in Semiconductors* (D. Van Nostrand Company, Inc., New York, 1950), p. 334.

[27] W. Hume-Rothery, *Structure of Metals and Alloys* (Institute of Metals Monograph, London, 1936).

[28] N. F. Mott and H. Jones, *The Theory of the Properties of Metals and Alloys* (Clarendon Press, Oxford, 1936).

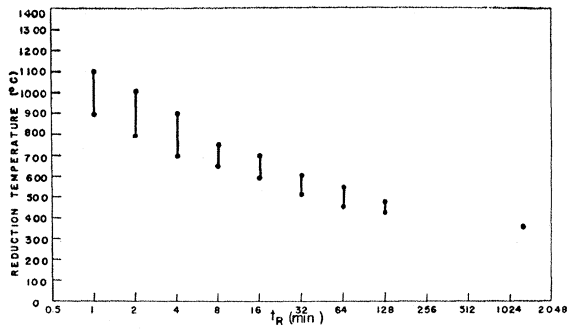

FIG. 26. Minimum time for uniform coloring of ceramic 10 mil sheet.

Strongly Reduced Ceramics

It is known that strong reduction of TiO_2 produces an *n*-type, blue-black, semiconductor which has an activation energy of *ca* 0.070 ev at room temperature in the 100 Ω^{-1} m^{-1} region.[6] This low activation energy indicates that, in this case, nearly all of the electrons are free to contribute to conduction at room temperature. The investigation of this conductivity region was made with ceramic samples.

Samples were reduced in a current of hydrogen in a controlled-temperature alundum furnace. The temperature of reduction was varied from 300° to 1150°C, and the depth of coloring noted after quenching to room temperature in nitrogen. Sheet samples[29] (10 mil) could be reduced uniformly at temperatures as low as 350°C (Fig. 26), although periods of the order of 24 hours were required; at 300°C, no observable reaction occurred in this length of time. In order to obtain uniformly reduced thin-sheet ceramic in times of the order of 5 minutes, it proved necessary to operate at temperatures above 700°C. For this reason most of the subsequent observations were carried out on materials reduced at 800°C in hydrogen.

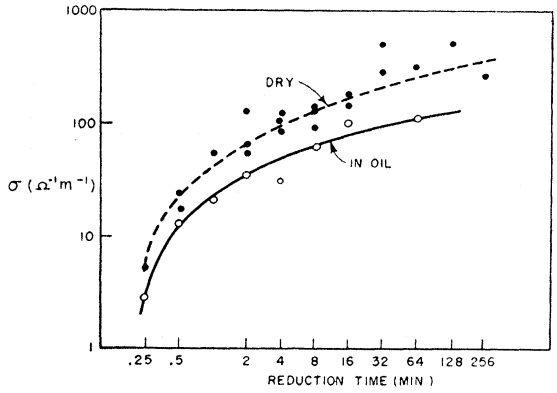

FIG. 27. Over-all conductivity *vs* reduction time for $\frac{1}{8}\times1\times0.01$ in. thin sheet samples.

[29] The samples were prepared from Tamco heavy grade rutile powder, partly in this Laboratory by J. Brownlow, and partly by courtesy of the Glenco Corporation, Metuchen, New Jersey.

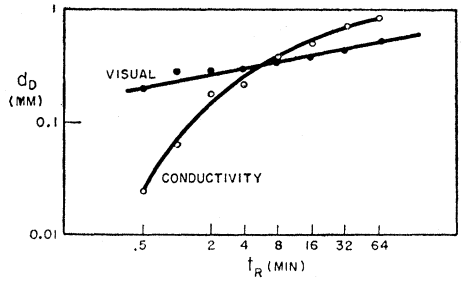

FIG. 28. "Diffusion distance" from visual observation of the "coloring distance" checked roughly by estimates from the over-all conductivity.

Nazu[30] has derived the chemical reaction constants for the reduction process $2TiO_2+H_2\rightarrow Ti_2O_3+H_2O$ over the temperature range 775° to 1000°C. The free energy change accompanying this process is $\Delta G^0 = 4095-2.013T\log_{10}T-3.86\times10^{-3}T^2+10.1T$. This equation predicts that ΔG^0 becomes zero at 324°C, a lower limit, which agrees fairly well with the experimental data just presented.

Some of the thin-sheet material showed a surprising anisotropy in reduction; the coloring appeared to move in from the edges of the sample as though the skin of the ceramic plate were impervious. At temperatures higher than 1100°C, a deposit of reduced TiO_2 is usually found on the furnace walls indicating that at these elevated temperatures the reduction process is rather violent.[6]

Measurements of the effective conductivity at room temperature for various times of reduction were made for $\frac{1}{4}$-in. cubes and 10-mil sheet ceramics. Copper electrodes were electroplated onto opposite ends of the samples after reduction and the resistance was determined by a Wheatstone bridge. These conductivity characteristics give a measure of the time required to reach the equilibrium concentration at 800°C. Figure 27 gives the conductivity characteristic for the sheet samples and Fig. 28 a comparison of a conductivity and visual penetration test on the cubes.

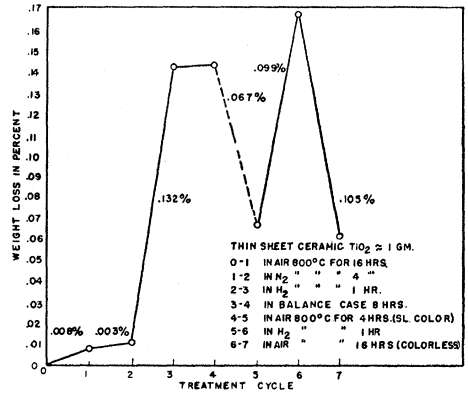

FIG. 29. Weight-loss experiment.

[30] N. Nazu, Science Repts Tôhoku Imp. Univ. 1, **25**, 510 (1936).

To establish the amount of oxygen lost during the reduction process, a ceramic sheet sample (10 mil, *ca* 1 g) was subjected to reduction-oxidation cycles and the weight change measured with a microbalance. The sample was initially heated in air at 800°C until its weight showed no further change (Fig. 29, point 1). The subsequent reduction and oxidation cycles are noted in the figure; it may be seen that for a reduction time of one hour at 800°C, a reversible weight loss of 0.1 percent is attained. At 650°C the weight loss in one hour amounts to 0.01 percent. Since only oxygen is lost from the lattice in this type of treatment, one can derive a simple formula for the number of conduction electrons as a function of the fractional weight loss δ: $n=3.17\times10^{26}\delta$ electrons/m^3 assuming that the loss of each oxygen atom leaves two electrons trapped

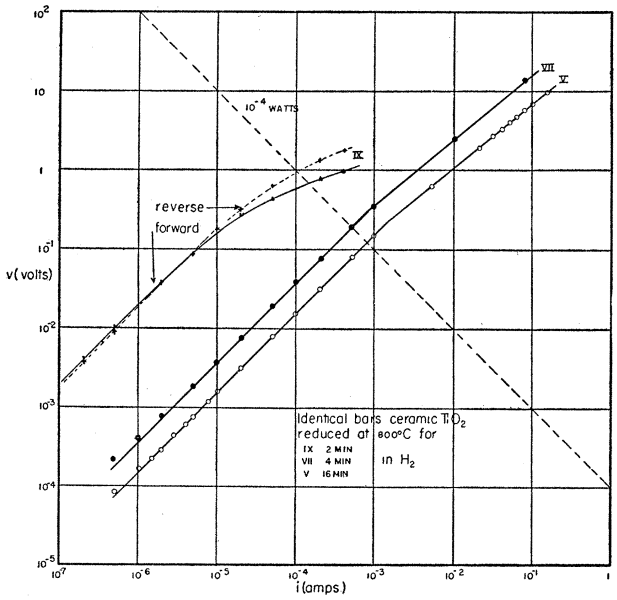

FIG. 30. Current-voltage curves for reduced ceramic bars.

at the resultant lattice vacancy. A weight loss of 0.1 percent should correspondingly release 3.17×10^{26} electrons/m^3 for conduction. Near one percent oxygen loss, the lattice tends to break down and the corundum structure of Ti_2O_3 begins to appear. Nazu[30] finds it impossible to reduce the material below Ti_2O_3 by hydrogen treatment, so that a valence of three for the titanium is the lowest that need be considered in the discussion of reduced TiO_2.[31]

Typical current-voltage curves are shown in Fig. 30. The resistance proves ohmic up to an applied field strength of about 10 v/m (0.1 volt). The deviation from Ohm's law seems to be connected, not with a particular power input, but occurs rather above a certain voltage. The heating could be neglected below a power input of 0.02 watt as comparison of oil and air

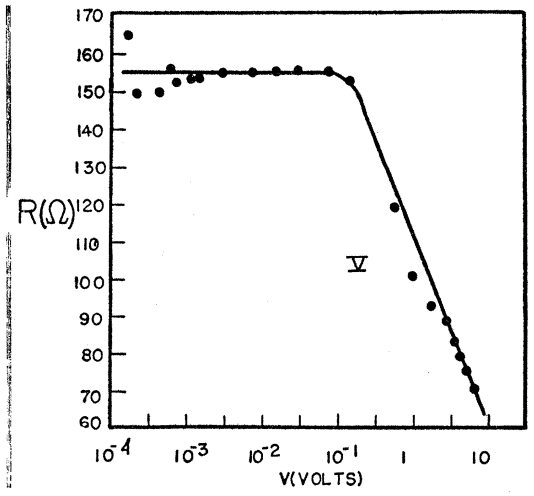

FIG. 31. Resistance as function of applied voltage.

cooling indicated, while the deviation from an ohmic behavior begins for a much smaller power input. Figure 31 gives a typical example of the rather sharp transition to a nonohmic behavior. This rapid change is tentatively identified with carrier injections; other evidence for this phenomenon has already been presented from photoconductivity and conductivity data.

The results of Hall-effect measurements, made with the arrangement previously used on a sheet sample reduced at 0.3 atmos hydrogen for 4 min at 800°C are shown in Fig. 32. One finds $V_H/B=8.88\times10^{-7}$ v-m^2/weber for the Hall constant $R=5.55\times10^{-8}$ m^3/coulomb, hence for the number n of charge carriers per unit volume, $(8/3\pi)(1/Re)=0.955\times10^{26}$ m^{-3}. From weight-loss experiments (1 hour reduction at 800°C gives 0.10 percent loss of weight corresponding to a conductivity

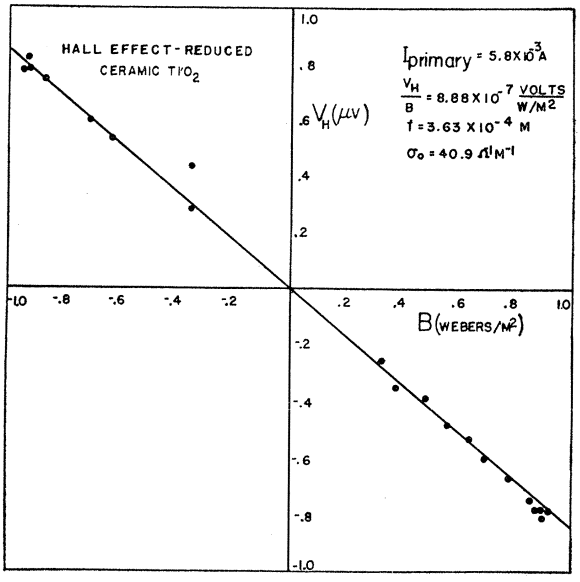

FIG. 32. Hall effect in reduced ceramic TiO_2.

[31] M. D. Earle, Phys. Rev. **61**, 56 (1942), assumes Ti^{+1}.

of 112 $\Omega^{-1}m^{-1}$), the concentration 1.2×10^{26} m^{-3} is calculated, which is in good agreement with this Hall value. For other samples a similar agreement was obtained.

The very high conductivity of the reduced ceramics, and the fact that the Hall measurement indicates that all of the electrons are free to contribute to conduction at room temperature, show that, in strongly reduced TiO_2 samples, the activation energy has become very low in agreement with earlier data obtained during the war in this Laboratory.[6]

ACKNOWLEDGMENT

The author gratefully acknowledges the continuous advice and encouragement received from Professor A. von Hippel in the course of this research. He is also greatly indebted to M. A. Gilleo for his help in the optical and photoelectric investigation; to W. B. Westphal and the Dielectric Measurements Group for assistance with ac conductivity measurements; and to Professor R. C. Lord and Professor L. Harris for their kindness in determining the infrared absorption in one of the crystals.

PHYSICAL REVIEW VOLUME 87, NUMBER 5 SEPTEMBER 1, 1952

Thermal Neutron Capture Cross Section of A^{40} and Observation of A^{42}†

SEYMOUR KATCOFF
Chemistry Department, Brookhaven National Laboratory, Upton, New York
(Received May 16, 1952)

The thermal neutron absorption cross section of A^{40} was determined by measuring in calibrated proportional counters the amount of 110-min A^{41} produced from samples of argon irradiated in a neutron flux whose magnitude was measured by β-γ coincidence counting of gold monitors. The result was 0.53 ± 0.03 barn.

A^{42} was produced from A^{40} by two successive neutron captures and it was detected through its 12.5-hr K^{42} daughter. A lower limit of 3.5 years was set on its half-life. From this result the thermal neutron absorption cross section of A^{41} is calculated to be greater than 0.06 barn.

It was also shown that the thermal neutron absorption cross section of A^{38} is 0.8 ± 0.2 barn.

INTRODUCTION

THE thermal neutron cross section of A^{40} for the formation of 110-min A^{41} was measured by Kern[1] and by Wattenberg and West.[2] They found values of 1.24 barns and 0.72 barn, respectively. In both cases the activity was measured by placing the argon in a cell external to a Geiger counter. At about the same time the total neutron absorption cross section of argon was measured by the "danger coefficient" method[3] using cadmium wire of known length and diameter as standard. This value, which also measures an upper limit for the activation cross section of A^{40}, was 0.62 barn. In a similar experiment Colmer and Littler[4] used the pile oscillator at Harwell and obtained the same value, 0.62 ± 0.04 barn. The total thermal neutron cross section (absorption plus scattering) for argon was first determined by Carroll[5] from transmission measurements. He used a Rn-Be in paraffin source and an argon sample which transmitted 92 percent of the neutron beam. His value was 2.5 barns. Melkonian *et al.*,[6] employed the Columbia University slow neutron velocity spectrometer and a sample of argon which transmitted 79 percent of the beam at 0.025 ev. Their result for the total cross section was 1.4 barns. If one subtracts from this the thermal neutron scattering cross section of 0.80 ± 0.08 barn determined by Harris[7] one obtains 0.6 barn for the absorption cross section, in good agreement with the direct measurements.[3,4]

In the present work the thermal neutron activation cross section of A^{40} was determined by measuring the A^{41} activity within a proportional counter and measuring the neutron flux by coincidence counting of gold

TABLE I. Activity per cc as function of counter length.

Length of cathode (cm)	Total counter volume (cc)	Cathode volume (cc)	Activity at a given time (counts/min)	Activity per cc of cathode volume (counts/min)
7.0	31.8	19.0	3460	182
17.0	59.6	47.1	8400	178
29.7	98.5	85.0	15,700	185
29.8	101.6	87.6	16,000	183
45.2	137.7	125.7	23,700	189
75.8	222.2	211.0	38,600	183
Average				183 ± 4

† Research carried out under the auspices of the AEC.

[1] B. D. Kern, unpublished Plutonium Project Report CP-772 (1943).

[2] A. Wattenberg and J. West, unpublished Plutonium Project Report CP-781 (1943).

[3] Lichtenberger, Fowler, and Wattenberg, unpublished Plutonium Project Report CP-781 (1943).

[4] F. C. W. Colmer and D. J. Littler, Proc. Phys. Soc. (London) **A63**, 1175 (1950).

[5] H. Carroll, Phys. Rev. **60**, 702 (1941).

[6] Melkonian, Rainwater, Havens, and Dunning, Phys. Rev. **73**, 1399 (1948).

[7] S. P. Harris, Phys. Rev. **80**, 20 (1950).